Integer wavelet transformations with predictive coding improves 3-D similar image set compression

Xiaojun Qi[a], John M. Tyler[a] and Oleg S. Pianykh[b]

[a]Computer Science Department, Louisiana State University, Baton Rouge, LA 70803
[b]School of Medicine, Department of Radiology, Louisiana State University, New Orleans, LA 70112

ABSTRACT

Lossless compression techniques are essential in archival and communication of large amounts of homogeneous data in radiological image databases. This paper exploits dependencies that exist between the pixel intensities in three dimensions to improve compression for a set of similar medical images. These 3-D dependencies are systematically presented as histograms, plots of wavelet decomposition coefficients, feature vectors of wavelet decomposition coefficients, entropy and correlation. This 3-D dependency is called set redundancy for medical image sets. Predictive coding is adapted to set redundancy and combined with integer wavelet transformations to improve compression. This set compression improvement is demonstrated with 3-D sets of magnetic resonance (MR) brain images.

Keywords: Predictive coding, integer wavelet transform, entropy coding and set redundancy

1. INTRODUCTION

The trend in medical imaging is toward direct digital image acquisition. This results in large amounts of homogeneous data in radiological image databases. An example of this is the multiple slices representing different cross sections of a body part being imaged. These are generated in a single procedure with commonly used modalities such as magnetic resonance imaging (MRI), computed tomography (CT), positron emission tomography (PET) and single-photon emission computed tomography (SPECT). Multiple slices are sometimes referred to as a 3-D image dataset. Storage and transmission of these large data sets require efficient data compression.

Data compression techniques can be broadly classified into lossy and lossless techniques. Lossy techniques can achieve a compression ratio of 50:1 or higher since they allow degradation, whereas lossless techniques can completely recover the original image with the tradeoff being a lower compression ratio of around 2:1.

Although lossy compression is often acceptable, lossless compression is sometimes preferred.[1] For instance, medical professionals prefer lossless compression since it facilitates accurate diagnosis with no degradation of the original images. Lossy compression techniques can lead to errors in diagnosis because of unknown artifacts introduced in compensation for a higher compression ratio. Furthermore, there exist legal and regulatory issues that favor lossless compression in medical applications. Similar issues exist for 3-D medical image data.

Because 3-D image data can be represented as multiple 2-D slices, it is possible to compress these 2-D images independently on a slice-by-slice basis by applying either the new lossless image compression standard JPEG-LS[2] or the context-based adaptive lossless image codec (CALIC) algorithm.[3] However, such an approach does not exploit dependencies that exist between pixel values in all three dimensions, especially in the temporal dimension. A better approach is to consider the whole set of slices as a single 3-D data set and exploit dependencies in all three dimensions. Several methods based on this approach have been proposed.[4-10] Some of these methods[4-8] use the 3-D discrete wavelet transform in a lossy compression scheme, whereas others[9, 10] use predictive coding and a lossless scheme. In a very recent paper[11], a 3D context-based embedded zerotree wavelet (CB-EZW) algorithm was proposed to efficiently encode 3-D image data exploiting the dependencies in all dimensions, while enabling lossy and lossless decompression from the same bit stream.

From our observation, most present 3-D image compression techniques either utilized 3-D discrete wavelet transforms or predictive coding, but not both. In this paper, we introduce a new technique that combines these to improve compression.

The remainder is organized as follows:

- Section 2 briefly introduces the concept of integer wavelet transform, which is a discrete wavelet transform in a lossless compression scheme.
- Section 3 briefly introduces the concept of predictive coding from both intra-frame and inter-frame points of view.
- Section 4 introduces the concept of set redundancy to exploit dependencies that exist between the pixel intensities in three dimensions from a new perspective.
- Section 5 proposes a practical implementation of set redundancy using predictive coding combined with integer wavelet transformations to improve compression.
- Section 6 discusses the compression results of 3-D sets of brain images obtained with the proposed compression method.
- Section 7 presents conclusions.

2. INTEGER WAVELET TRANSFORM

2.1 Wavelet based compression technique

One use of wavelet transformations is to represent functions as a superposition of a wavelet basis.[12-14] The coefficients of the basis can be used to exactly reconstruct the original function. Dilation and translation of a special function, which is called the mother wavelet, form the wavelet basis. The wavelet transform provides both spatial and frequency representation of signals. The application of wavelet transforms in image compression has shown promising results.[15-21]

Figure 1 presents the block diagram of two levels of a 1-D wavelet compression process.

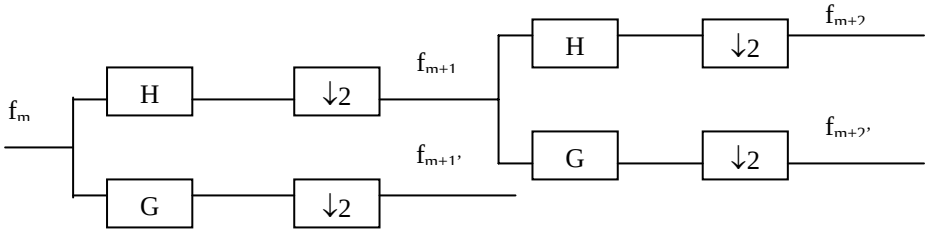

Figure 1 Two levels of the 1-D wavelet compression process.

Wavelet transforms can be implemented with perfect reconstruction finite impulse response (FIR) filter banks.[22, 23] Figure 2 shows a two-channel filter bank, where $\tilde{H}$ and $\tilde{G}$ are analysis filters and H and G are synthesis filters.

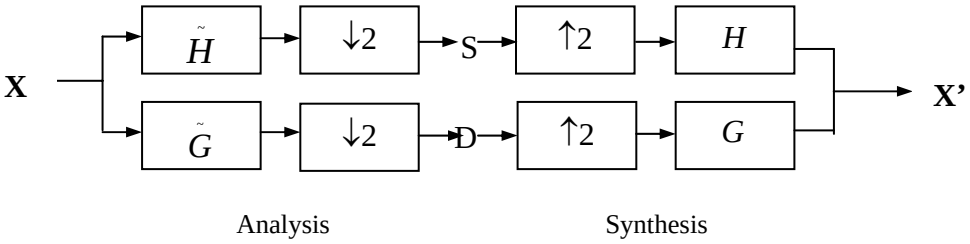

Figure 2 Analysis and synthesis filter banks.

If the filters selected are such that:

$$H(z)\tilde{H}(z) + G(z)\tilde{G}(z) = 2z^{-1} \qquad (1)$$

$$H(z)\tilde{H}(-z) + G(z)\tilde{G}(-z) = 0 \qquad (2)$$

a filter bank has perfect reconstruction with a delay of *l*.

The wavelet transform is theoretically lossless because many wavelet transformations are theoretically reversible. However, in practice, wavelets have floating-point coefficients and computers have only finite precision floating-point calculations, so some data maybe lost through "truncation". This limitation of finite precision arithmetic causes the wavelet based lossless compression to be less desirable.

Lossless image compression is very important for images in medical and space science applications. In these, the compression algorithm always compresses the information as much as possible and avoids losing any information. As a result, we propose using a general integer coefficient wavelet reversible transformation, which is referred to as lifting, to avoid losing any information.

2.2 Lifting – the second generation wavelets

Lifting is a relatively new method for constructing wavelets. The difference compared to classical wavelet construction is that it does not rely on the Fourier transform.[24-27] Lifting is used to construct second-generation wavelets, which are not necessarily translations and dilations of one function. It has been proven by Daubechies and Sweldens[28] that any discrete wavelet transform can be computed using lifting, and these transforms also reduce computational complexity when compared to classical filtering algorithms.

Lifting consists of three main steps:

- **Split**: Split reduces the number of coefficients representing a signal by sub-sampling the even samples and obtaining a new sequence. That is, the original data is sub-sampled into odd and even sets.
- **Predict**: Predict constructs a prediction operator ρ, which is typically based on a model of the signal data, to predict the missing parts from **Split** step. It determines the wavelet coefficients through a failure to predict the odd set based upon the even set. This step is also referred to as the **Dual Lifting** step.
- **Update**: This step updates the even set using the wavelet coefficients already determined to compute the scaling function coefficients, which maintains the needed properties among all the wavelet coefficients at all levels. This step is also referred to as **Lifting** step.

Figure 3 illustrates the iterated process using *M* pairs of "predict" and "update" to perform lifting.

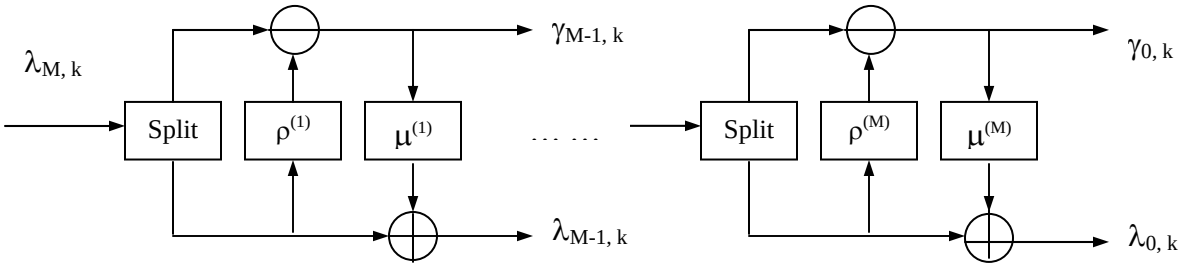

Figure 3 The forward *M*-level wavelet transform using *M* pairs of dual lifting (predict) and lifting (update).

2.3 Integer wavelet transforms

Through lifting, an integer version of every floating-point wavelet transform can be obtained. Integer wavelet transforms, i.e., wavelet transforms that transform integers to integers, can be developed using lifting by rounding the result of each dual lifting and lifting step before adding or subtracting. The forward and inverse transforms that generate integers in each step are demonstrated below. An in-place implementation can be easily derived from these diagrams and equations.

The three stages of lifting are combined and iterated to generate the 1-D lifted fast forward wavelet transform algorithm. Once the forward transform is obtained, the inverse can be immediately derived by reversing the lifting and the dual lifting steps and flipping the signs.

for $j := -1$ *downto* $-n$

$\{\lambda_{j,k}, \gamma_{j,k}\} := Split(\lambda_{j+1,k})$

$\gamma_{j,k} = \gamma_{j,k} - \lfloor \rho(\lambda_{j,k}) + 1/2 \rfloor$

$\lambda_{j,k} = \lambda_{j,k} + \lfloor \mu(\gamma_{j,k}) + 1/2 \rfloor$

end

(a) 1-D lifted fast forward wavelet transform

for $j := -n$ *to* -1

$\lambda_{j,k} = \lambda_{j,k} - \lfloor \mu(\gamma_{j,k}) + 1/2 \rfloor$

$\gamma_{j,k} = \gamma_{j,k} + \lfloor \rho(\lambda_{j,k}) + 1/2 \rfloor$

$\{\lambda_{j+1,k}\} = Join(\lambda_{j,k}, \gamma_{j,k})$

end

(b) 1-D lifted fast inverse wavelet transform

Figure 4 Forward and inverse integer wavelet transform.

3. PREDICTIVE CODING[29]

3.1 Inter-image prediction

Inter-image prediction assumes that high image correlation alone implies image similarity. Consequently, high correlation among several images means that the images are almost linearly dependent, i.e., some part of the image can be efficiently predicted with linear combinations of the others. If $V = \{v_1, v_2, \ldots, v_n\}$ is a set of similar images v_i and each v_i is highly correlated with the other images in the set represented as $V^{(i)} = V \backslash \{v_i\}$. Then v_i can be expressed as:

$$v_i = \left\lfloor \sum_{j \neq i,\, j=1}^{j=n} \beta_j v_j \right\rfloor + r^{(i)} = \lfloor \beta^{(i)} V^{(i)} \rfloor + r^{(i)} = \hat{v}_i + r^{(i)}$$

for lossless similar images compression, where $\lfloor \ \rfloor$ represents integer truncation. Both coefficients $\beta^{(i)}$ and compressed residual $r^{(i)}$ are stored to completely recover v_i.

3.2 Inter-image prediction with region matching

Inter-image prediction is improved when each pixel in image u is not predicted from the similar overlapped region of the image v, but from the region in v which has the closest intensity match to some neighborhood of u.

3.3 2D and 3D autogressive (AR) models

This technique, also known as differential pulse code modulation (DPCM), includes image shifts in the predictive model because neighboring pixels tend to have close, i.e., correlated, intensity values in any image. Therefore, a pixel intensity may be predicted from the intensities of its surrounding pixels. The AR model of the k-th order for the 2-D image *u[i, j]* is

$$u[i, j] = \left\lfloor \sum_{m=1}^{k} \beta_m u[i - a_m, j - b_m] \right\rfloor + r = \left\lfloor \sum_{m=1}^{k} \beta_m B^{a_m} L^{b_m} u \right\rfloor + r = \lfloor \beta u_s[i, j] \rfloor + r$$

where β_m, a_m and b_m are optimally chosen constants (a_m and b_m are integers) and u_s is for all left and bottom shifts of the image u used in a particular model.

2-D models can be extended to 3-D models which include inter-image relations. The AR model of the k-th order for the 3-D image is:

$$u = \left\lfloor \sum_{j} \alpha_j v_j + \sum_{m=1}^{k} \beta_m B^{a_m} L^{b_m} u \right\rfloor + r = \left\lfloor \beta u_s + \sum_{j} \alpha_j v_j \right\rfloor + r$$

where v_j are images similar to u. When all v_j represent close slices of the same 3-D object, this model efficiently decorrelates the data.

Predictive coding in 3-D image data makes an estimate for the value of the current pixel based on previous values for that location and other neighboring areas. The rules for estimating are stored in the decoder and, for any new pixel, the encoder need only send the difference value between what the rules have predicted and the actual value of the new element. The more accurate the prediction, the less data sent.

4. SET REDUNDANCY IN 3-D SIMILAR IMAGES

In this section, 20 slices comprising an example MR brain volume with 256*256 pixels in each single slice are used to demonstrate the spatial redundancy in 3-D similar image sets.

MRI is used to image physical structures in anatomies. MRI systems produce brain images in cross-sections. These brain images are acquired by measuring the interaction between pulses of radio frequency (RF) radiation and tissues in a strong magnetic field. Then they are transformed to reconstruct a "3-dimensional" digital image volume. Figure 5 depicts a 20 MR brain slice example.

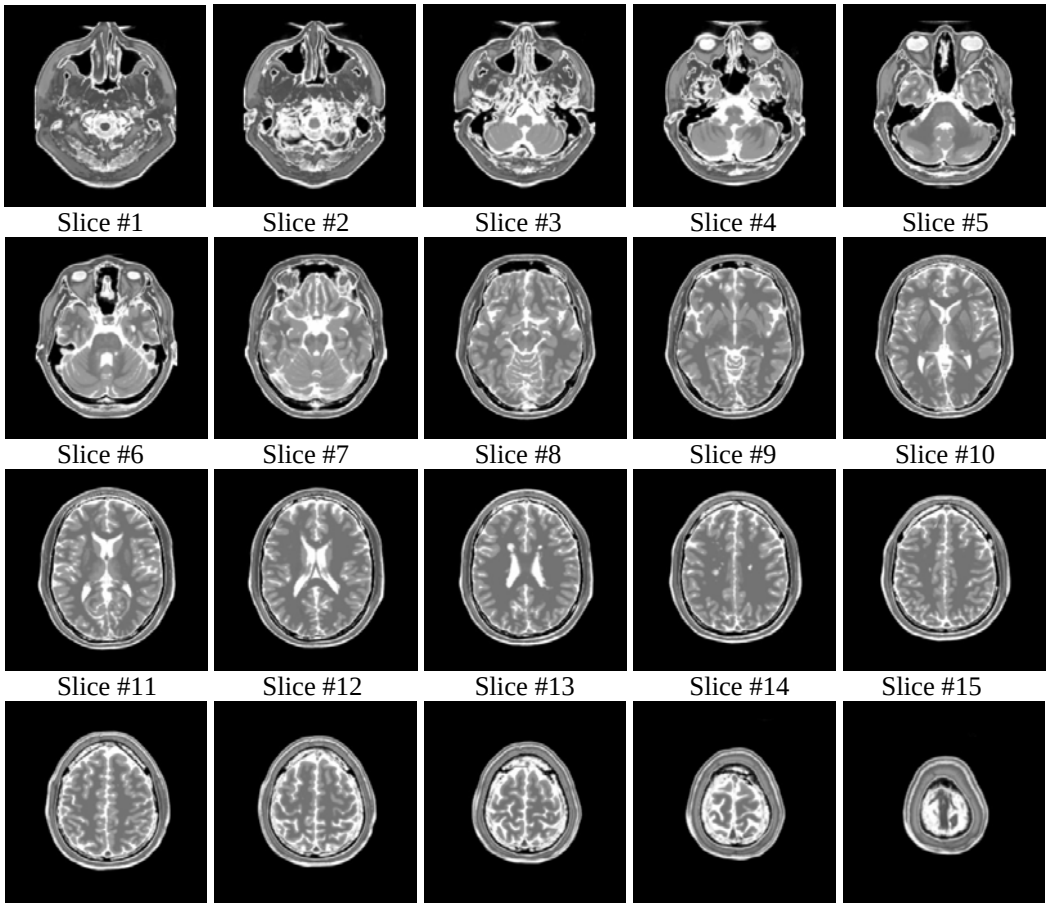

Figure 5 20 slices of MR brain images comprising an example volume.

4.1 Spatial redundancy in a 3-D MR brain image set

MRI data contain large quantities of noise, which are uncorrelated from slice to slice. This causes the structure of the cross dependence to be more complicated than temporal sequences. Yet, a significant amount of redundancy between successive MR slices can be found after a close investigation of the structure of the resultant brain images (Figure 5). For example, they are similar in terms of the shape, pixel intensity at a certain anatomical position, and analogous anatomical structures are observed from subjective observations. Statistical analysis was also done to further illustrate the similarity of these images.

Histogram Analysis

Histograms for several nonadjacent MR brain slices from Figure 5 are presented on Figure 6. Figure 6 shows that more than 50 percent of the pixels have zero intensity (100 percent black) and all the other intensities are uniformly distributed with all being less than 10 percent.

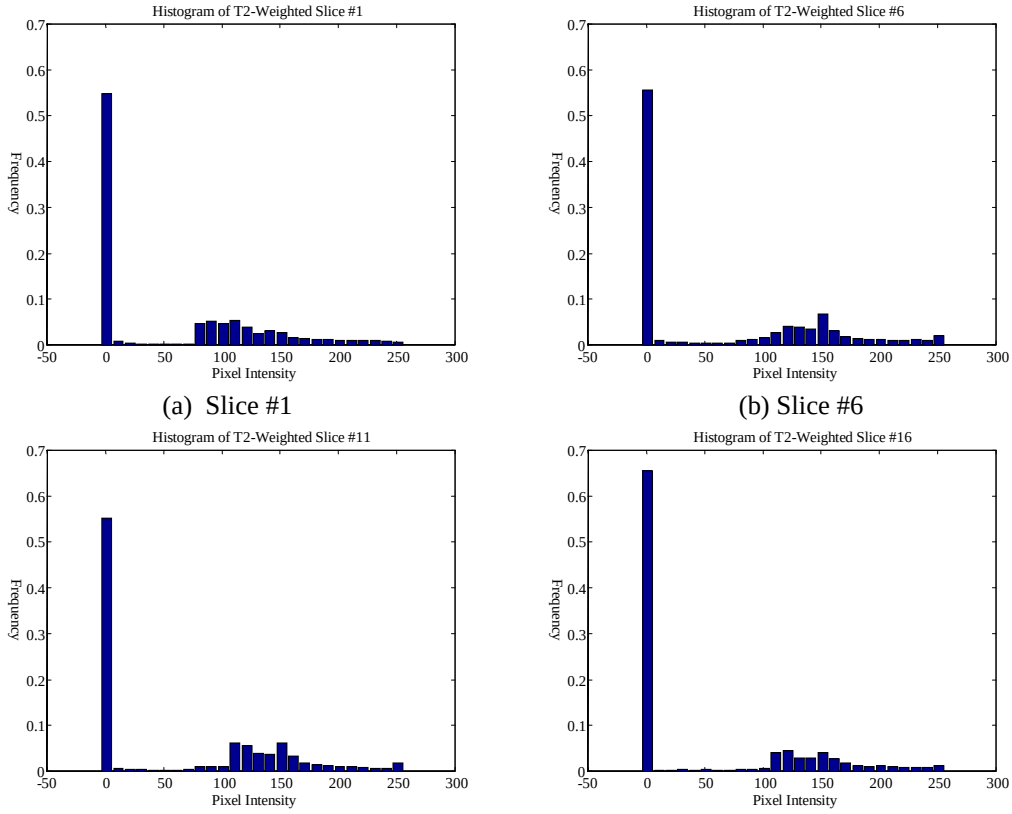

(a) Slice #1 (b) Slice #6

(c) Slice #11 (d) Slice #16

Figure 6 Comparable histograms of four nonadjacent MR brain slices (Figure 5).

Plot of Wavelet Coefficients

A two-level wavelet transform was applied to the same four nonadjacent MR brain slices presented on Figure 6. The plots of all decomposed sub-image coefficients for all four slices are presented on Figure 7. *A2*, *H2*, *V2*, *D2*, *H1*, *V1* and *D1* represent level 2 and level 1 wavelet transform decompositions for the average, horizontal, vertical and diagonal respectively. The abscissa represents the vector position and the ordinate represents the value of the decomposed coefficients in their corresponding vector position. All four slices have very similar (not identical) plots for the level 2 average decomposition, which is a coarse approximation of the original slice at a high scale, as shown on each subplot *A2*. Deviations from the average approximation for the horizontal, vertical and diagonal are also similar to each other.

Feature Vector

Table 1 lists the mean and variance for all decomposed sub-images presented on Figure 7. The corresponding vectors *(MA_2, VA_2, MH_2, VH_2, MV_2, VV_2, MD_2, VD_2, MH_1, VH_1, MV_1, VV_1, MD_1, VD_1)* derived from the first row of Table 1 are defined as feature vectors since both the mean and the variance are good statistical measure to represent the general characteristics of this population. MA_2, MH_2, MV_2, MD_2, MH_1, MV_1 and MD_1 respectively represent the level 2 and level 1 means for wavelet decompositions of average, horizontal, vertical and diagonal, where VA_2, VH_2, VV_2, VD_2, VH_1, VV_1 and VD_1 represent these corresponding variances. There are only slight deviations in the feature vectors of these four MR brain slices.

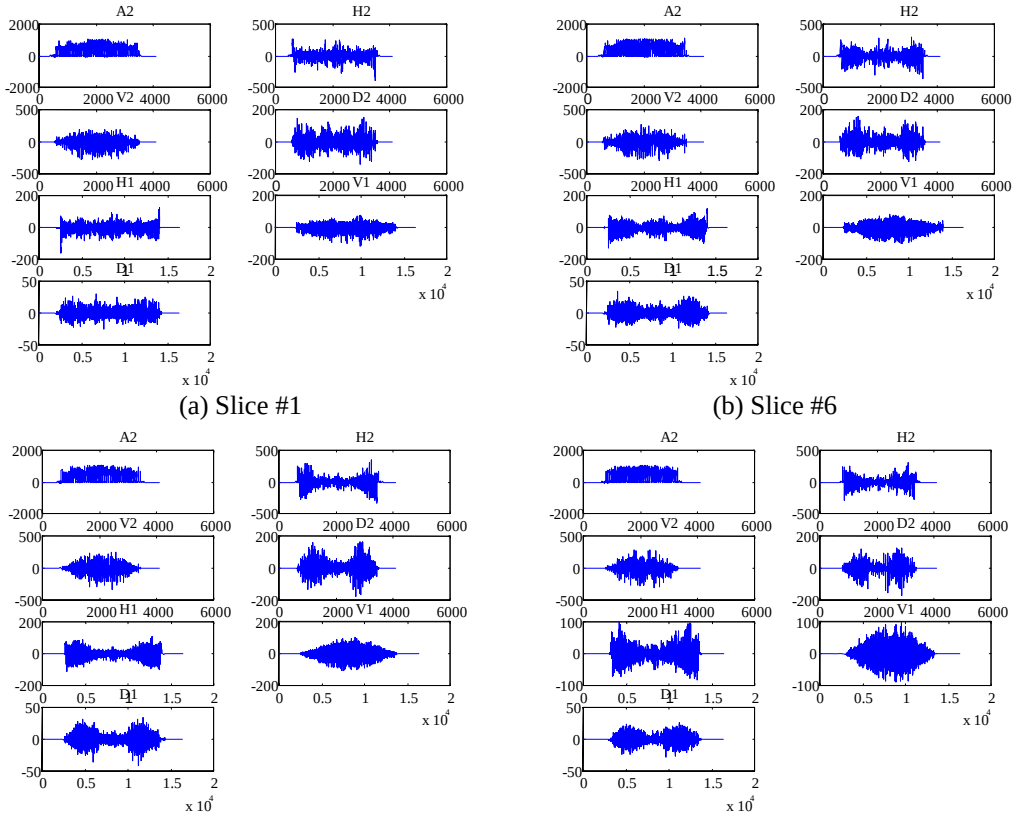

(a) Slice #1 (b) Slice #6

(c) Slice #11 (d) Slice #16

Figure 7 Coefficients of decomposed sub-images for a 2-level wavelet transform.

	MA_2	VA_2	MH_2	VH_2	MV_2	VV_2	MD_2	VD_2	MH_1	VH_1	MV_1	VV_1	MD_1	VD_1
#1	229.51	277.52	0.94	41.93	-0.37	38.50	0.02	20.03	-.06	12.89	-0.04	9.78	.003	2.87
#6	256.90	313.32	0.03	46.70	0.26	40.61	-.11	19.69	0.05	12.78	0.002	10.90	-.003	3.00
#11	255.57	302.37	0.11	47.84	-0.13	37.13	-.05	21.30	-.0003	13.09	-.003	11.28	-.008	3.38
#16	204.11	296.00	0.03	38.94	0.008	37.45	-.05	17.73	-.01	10.52	0.003	9.79	0.006	2.78

Table 1 Feature vector for four nonadjacent MR brain slices

Entropy

The entropy for the four nonadjacent MR brain slices and their corresponding wavelet transform images are shown in Table 2. The entropy of an image is a measure of the information an image contains, and it is also used as a measure of the compressibility of the image (lower entropy means better compressibility). The comparable entropy values for all four MR brain slices illustrate that each contains an almost equal amount of information. This holds for the wavelet transform entropy.

Slice	Original Entropy	WT Entropy
Slice #1	4.5501	3.9201
Slice #6	4.5068	3.8518
Slice #11	4.3363	3.6906
Slice #16	3.5683	3.1110

Table 2 Entropy and wavelet transform entropy for four nonadjacent MR brain slices from the image sets.

Correlation

The correlation was determined (Table 3) between these same four nonadjacent MR brain slices. The existence of a statistical correlation between two slices can be verified numerically by calculating the correlation coefficient. For the four nonadjacent MR brain slices, which should have less similarity than adjacent slices, the correlation was between 0.6 and 0.8. There were similarities among these four slices but there was even more similarity with adjacent MR brain slices.

Correlation	Slice #1	Slice #6	Slice #11	Slice #16
Slice #1	1	0.7311	0.7663	0.6272
Slice #6	0.7311	1	0.7953	0.6438
Slice #11	0.7663	0.7953	1	0.7213
Slice #16	0.6272	0.6438	0.7213	1

Table 3 Correlation between all four nonadjacent MR brain slices.

4.2 Summary

Based on these statistical analyses, we concluded that the redundancies in this 3-D MR brain image set can be summarized as follows:

- Similar pixel intensities in the same areas,
- Similar edge distributions,
- Analogous distributions of features,
- Comparable histograms (Figure 6),
- Identical sub-image coefficients of each decomposition and comparable feature vectors after applying wavelet transforms (Figure 7 and Table 1),
- Comparable entropy for both original images and wavelet transformed images (Table 2),
- High correlation (Table 3).

The spatial redundancies in a 3-D MR brain image set may be expanded to other 3-D medical image sets.

It has been proven[30] that entropy of the image set will decrease when the redundancies of the same image set increases. Therefore, we can utilize the set redundancy in a 3-D medical image set to further the compression.

5. IMPLEMENTATION

The algorithm we developed for 3-D medical image set compression is a combination of predictive coding, integer wavelet transform and entropy coding. Figure 8 shows the block diagram of the 3D compression algorithm.

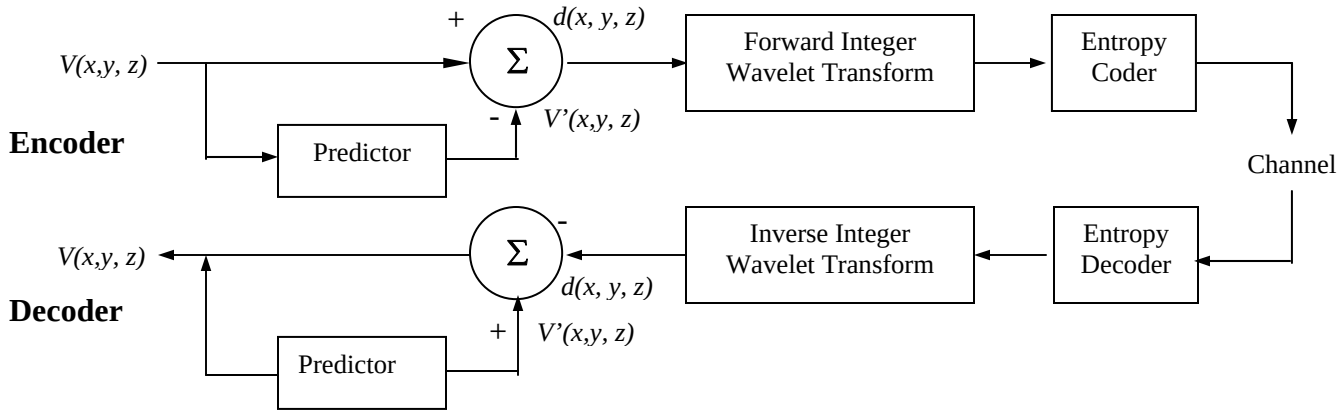

Figure 8 Block diagram of the 3-D medical image set compression algorithm.

5.1 The predictor

In a 3-D medical image set, adjacent slices usually possess a higher degree of spatial coherence than nonadjacent ones. Predictive coding exploits this spatial coherence to calculate an intensity value from the previously encoded slices. The difference between the predicted intensity value and the actual intensity value of the current slice is encoded since the entropy of the prediction errors is normally lower than that of the original image. Thus transmission of the prediction error is more efficient than transmission of the original image.

We assume that the 3-D medical image set, $V(x, y, z)$, is a wide-sense stationary random process. The predictor is of the following form:

$$V'(x, y, z) = a_1V(x-1, y, z) + a_2V(x, y-1, z) + a_3V(x, y, z-1)$$

where $V(x-1, y, z)$, $V(x, y-1, z)$ and $V(x, y, z-1)$ are 1-pixel shifts of the image set V in x, y and z direction respectively. That is, the predictor is causal since it is formed from values which have already been processed. The decoder can track the operation of the encoder and generate the same predicted values as the encoder due to this causality.

The predictor coefficients $A = (a1, a2, a3)$ are determined so that the predictor is optimal with respect to mean-square-error (MSE). To be optimal, the predictor must minimize the variance of the predicted errors $\varepsilon(x, y, z) = V(x, y, z) – V'(x, y, z)$. That is, to minimize $E[\varepsilon^2(x, y, z)]$, where $E[.]$ is the probabilistic expectation operator. This minimization occurs when the error is orthogonal to the slices upon which the prediction is based:

$$E[\varepsilon(x, y, z)v(x-1, y, z)] =0 ;$$
$$E[\varepsilon(x, y, z)v(x, y-1, z)] = 0 ;$$
$$E[\varepsilon(x, y, z)v(x, y, z-1)]= 0 .$$

After some algebra, $A = P*(R^{-1})$ is derived where $R = E[X^TX]$, $P = E[I(r)X]$, X denotes the predicted image, $I(r)$ denotes the training image, and $E[.]$ denotes expected value, over all r.

5.2 Integer wavelet transforms

A family of symmetric, biorthogonal wavelets can be constructed from interpolating Deslaurriers-Dubuc scaling functions[31] by varying the three lifting stages, as:

1. Choose different wavelets, other than the lazy wavelets, for the initial split.
2. Choose a different number of vanishing moments (N) of the dual wavelet, i.e., analyzing high pass filter.
3. Choose a different number of vanishing moments ($\tilde{N}$) of the primal (real) wavelet, i.e., synthesizing high pass filter.

Here, the following different sets of $(N, \tilde{N})$ was used to conduct both the forward and inverse integer wavelet transformation.[32]

- **(2, 2) interpolating transform:**

$$d_{1,l} = s_{0,2l+1} - \lfloor 1/2(s_{0,2l} + s_{0,2l+2}) + 1/2 \rfloor$$
$$s_{1,l} = s_{0,2l} + \lfloor 1/4(d_{1,l-1} + d_{1,l}) + 1/2 \rfloor$$

- **(4, 2) interpolating transform:**

$$d_{1,l} = s_{0,2l+1} - \lfloor 9/16(s_{0,2l} + s_{0,2l+2}) - 1/16(s_{0,2l-2} + s_{0,2l+4}) + 1/2 \rfloor$$
$$s_{1,l} = s_{0,2l} + \lfloor 1/4(d_{1,l-1} + d_{1,l}) + 1/2 \rfloor$$

- **(2, 4) interpolating transform:**

$$d_{1,l} = s_{0,2l+1} - \lfloor 1/2(s_{0,2l} + s_{0,2l+2}) + 1/2 \rfloor$$
$$s_{1,l} = s_{0,2l} + \lfloor 19/64(d_{1,l-1} + d_{1,l}) - 3/64(d_{1,l-2} + d_{1,l+1}) + 1/2 \rfloor$$

- **(6, 2) interpolating transform:**

$$d_{1,l} = s_{0,2l+1} - \lfloor 75/128(s_{0,2l} + s_{0,2l+2}) - 25/256(s_{0,2l-2} + s_{0,2l+4}) + 3/256(s_{0,2l-4} + s_{0,2l+6}) + 1/2 \rfloor$$
$$s_{1,l} = s_{0,2l} + \lfloor 1/4(d_{1,l-1} + d_{1,l}) + 1/2 \rfloor$$

- **(4, 4) interpolating transform:**

$$d_{1,l} = s_{0,2l+1} - \lfloor 9/16(s_{0,2l} + s_{0,2l+2}) - 1/16(s_{0,2l-2} + s_{0,2l+4}) + 1/2 \rfloor$$
$$s_{1,l} = s_{0,2l} + \lfloor 9/32(d_{1,l-1} + d_{1,l}) - 1/32(d_{1,l-2} + d_{1,l+1}) + 1/2 \rfloor$$

5.3 Entropy coding

Huffman coding, LZ (Lempel-Ziv) coding and arithmetic coding are the commonly used entropy coding schemes. We used the Unix utilities compress and pack for entropy coding. Compress is based on Adaptive Lempel-Ziv (ALZ) method and commonly used for lossless compression of images and other data. Pack uses Huffman coding. We also used a more sophisticated entropy coding method, which uses arithmetic coding as implemented by Alistair Moffat.[33]

6. EXPERIMENTAL RESULTS

Table 4 compares the compression performance of our 3-D compression algorithm applying different biorthogonal wavelets constructed from interpolating Deslaurriers-Dubuc scaling functions, the Unix utilities compress and pack, and arithmetic coding.

3D Image Set	$(N, \tilde{N})$	Best %Comp/ Ratio	Data Size (Bytes)	Compress	Pack	Arithmetic Coding
				Size/%comp/ratio	Size/%comp/ratio	Size/%comp/ratio
Original			1310720	554931/57.66%/2.36	669808/48.90%/1.96	664004/49.34%/1.97
Predicted		63.99%/2.78	1310757	471965/63.99%/2.78	553504/57.77%/2.37	546322/58.32%/2.40
2-Level Predicted Integer Wavelet Transform	(2, 2)	(6, 2) Compress 1311720 → 439977 66.46%/2.98	1311178	445903/65.99%/2.94	493931/62.33%/2.65	486701/62.88%/2.69
	(4, 2)		1311346	440097/66.44%/2.98	490286/62.61%/2.67	483335/63.14%/2.71
	(2,4)		1311406	448903/65.77%/2.92	496743/62.12%/2.64	489656/62.66%/2.68
	(6,2)		1311394	**439977/66.45%/2.98**	490868/62.57%/2.67	484076/63.09%/2.71
	(4, 4)		1311418	440840/66.38%/2.97	491094/62.55%/2.67	484218/63.08%/2.71
3-Level Predicted Integer Wavelet Transform	(2, 2)	(4,2) Compress 1311720 → 445943 66.00%/2.94	1311484	451171/65.50%/2.91	496568/62.14%/2.64	489648/62.66%/2.68
	(4, 2)		1311604	**445943/66.00%/2.94**	493773/62.35%/2.66	487142/62.86%/2.69
	(2,4)		1311730	454277/65.37%/2.89	499177/61.95%/2.63	492408/62.46%/2.66
	(6,2)		1312072	449655/65.73%/2.92	496854/62.13%/2.64	490502/62.62%/2.67
	(4, 4)		1311670	446035/65.99%/2.94	493835/62.35%/2.66	487226/62.85%/2.69

Table 4 Comparison of compression and compression ratios of
different level integer wavelet transforms and different entropy codings on 3-D MR brain image set

Since the differences between the predicted value and the actual value and the range of intensities after integer wavelet transform can be expanded, the predicted image set and the predicted integer wavelet image set are increased as shown in Table 4.

Observations made from Table 4:

- Wavelet filters with more analyzing vanishing moments generally perform better than these with more synthesizing vanishing moments. For instance, the (6, 4) interpolating transform performs best with the level 2 decomposition and the (4, 2) interpolating transform performs best with the level 3 decomposition.
- The level 2 decomposition performs better than the level 3 decomposition for every $(N, \tilde{N})$ interpolating transform pair.
- Among the entropy coding schemes used, compress performs best and pack performs worst. That is, ALZ coding compresses the best, and Huffman coding the worst.

Table 5 presents the entropy, in terms of bpp (bit per pixel). It shows the original 3-D image set entropy (the entropy of $V(x, y, z)$), the entropy of the differences $d(x, y, z)$, the entropy of the predicted integer wavelet transformed image set and the average compression expressed as the average number of bits per pixel of the compressed 3-D image set applying compress,

pack and arithmetic coding. Note that the predictor reduces entropy; i.e., *d(x, y, z)* has less entropy than *V(x, y, z)*. Only the compress entropy coder produces an output that is, on average, 0.5 bpp above entropy of *d(x, y, z)*.

3D Image Set	$(N, \tilde{N})$	Entropy (bpp)	Compress	Pack	Arithmetic Coding
			Entropy	Entropy	Entropy
Original		4.0538	3.3870	4.0882	4.0528
Predicted		3.3349	2.8806	3.3783	3.3345
2-Level Predicted Integer Wavelet Transform	(2, 2)	2.9684	2.7218	3.0147	2.9706
	(4, 2)	2.9466	2.6861	2.9925	2.9500
	(2,4)	2.9851	2.7399	3.0319	2.9886
	(6,2)	2.9508	**2.6854**	2.9960	2.9546
	(4, 4)	2.9515	2.6907	2.9974	2.9554
3-Level Predicted Integer Wavelet Transform	(2, 2)	2.9844	2.7537	3.0308	2.9886
	(4, 2)	2.9685	**2.7218**	3.0138	2.9733
	(2,4)	2.9997	2.7727	3.0467	3.0054
	(6,2)	2.9867	2.7445	3.0326	2.9938
	(4, 4)	2.9686	2.7224	3.0141	2.9738

Table 5 Comparison of entropy

7. CONCLUSION

The dependencies (set redundancy) existing between the pixel intensities in three dimensions based on the histograms, wavelet decomposition coefficients plots, feature vectors, entropy and correlation were exploited. Then we presented an efficient method designed specifically for the compression of 3-D medical image data, which was demonstrated with 3-D sets of MR brain images. The method combines the predictive coding, which is adapted to the set redundancy, and the integer wavelet transform to improve compression. The optimal predictor designed for each slice in the 3-D MR brain image set assumes that the statistics are wide-sense stationary throughout the whole image set. Our method produces the highest compression ratio of 2.98 after applying ALZ entropy coding. One could obtain better predictions (and, thus, better compression) by designing a number of different predictors, each optimized to a particular slice of the set, rather than choosing one predictor for the entire set with a tradeoff of more computational complexity.

REFERENCES

1. S. Wong, L. zaremba, D. Gooden, and H. K. Huang, "Radiologic image compression – a review," *Proc. IEEE 83*, pp. 194—219, 1995.
2. M. J. Weinberger, G. Seroussi, and G. Sapiro, "LOGO-I: a low complexity, context-based lossless image compression algorithm," in *Proceedings of the 1996 IEEE Data Compression Conference* (Institute of Electrical and Electronics Engineers, New York, 1996), pp. 140—149, 1996.
3. X. Wu and N. Memon, "CALIC – a context based adaptive lossless image codec," in *Proceedings of the 1996 IEEE International Conference on Acoustic, Speech, and Signal Processing* (Institute of Electrical and Electronics Engineers, New York, 1996), pp. 1890-1893, 1006
4. J. Wang and H. K. Huang, "Medical image compression by using three-dimensional wavelet transformation," *IEEE Trans. Med. Imag.*, Vol. 15, pp. 547—554, 1996.
5. J. Luo, X. Wang, C. W. Chen, and K. J. Parker, "Volumetric medical image compression with three-dimensional wavelet transform and octave zerotree coding", in *Visual Communications and Image Proceeding '96*, R. Ansari and J. J. Smith, eds, Proc. SPIE 2727, 579—590 (1996).
6. M. A. Pratt, C. H. Chu, and S. Wong, "Volume compression of MRI data using zerotrees of wavelet coefficients," in *Wavelet Applications in Signal and Image Processing IV*, M.A. Unser, A. Aldroubi, and A. F. Laine, eds, Proc. SPIE 2825, pp. 752—763, 1996.
7. A. Baskurt, H. Benoit-Cattin, and C. Odet, "On a 3-D medical image coding method using a separable 3-D wavelet transform," in *Medical Imaging 1995: Image Display*, Y. Kim, ed., Proc. SPIE 2431, pp. 184—194, 1995.
8. J. A. Saghri, A. G. Tescher, and J. T. Reagan, "Practical transform coding of multispectral imagery," *IEEE Signal Process. Mag.*, Vol. 12, pp. 32-43, 1995.

9. B. Aiazzi, P. S. Alba, S. Baronti, and L. Alparone, "Three-dimensional lossless compression based on a separable generalized recursive interpolation," in *Proceedings of the 1996 IEEE International Conference on Image Processing* (Institute of Electrical and Electronics Engineers, New York, 1996), pp. 85—88, 1996.
10. K. L. Lau, W. K. Vong, and W. Y. Ng, "Lossless compression of 3-D images by variable predictive coding," in *Proceedings of the Second Singapore International Conference on Image Processing* (World Scientific, Singapore, 1992), pp. 161—165, 1992.
11. Ali Bilgin, George Zweig, and Michael W. Marcellin, "Three-dimensional image compression with integer wavelet transform", *Applied Optics*, Vol. 39, No. 11, pp. 1799 – 1815, April 2000.
12. S. G. Mallat, "A theory for multiresolution signal decomposition: the wavelet representation," *IEEE Trans. Pattern Anal. Machine Intell.*, Vol. 11, No. 7, pp. 674-693, June 1989.
13. Stephane Mallat and Wen Liang Hwang, "Singularity detection and processing with wavelets," *IEEE Trans. On Info. Theory*, Vol. 38, No. 2, March 1992.
14. I. Daubechies, "Orthonormal bases of compactly supported wavelets," *Comm. Pure Appl. Math*., Vol. 41, pp. 909-996, 1988.
15. M. Olhta, M. Yano and T. Nishitani, "Wavelet picture coding with transform coding approach," *IEICE Trans. Fundamentals*, Bol. E75-A, No. 7, pp. 776-785, 1992.
16. J. N. Bradley, and M. Brislawn, "The wavelet/scalar quantization compression standard for digital fingerprint images," *Proc. IEEE ISCA-94*, London, 1994.
17. M. Antonini, M. Barland, P. Mathieu, and I. Daubechies, "Image coding using wavelet transform," *IEEE Trans. Image Processing*, Vol. 1, pp. 205-220, 1992.
18. John W. Woods, editor, *Subband Image Coding*, The Kluwer international series in engineering and computer science, Kluwer Academic Publishers, Norwell, MA, 1991.
19. J. Wang and H. K. Huang, "Three-dimensional medical image compression using a wavelet transform with parallel computing," *SPIE Med. Image*, Vol. 2431, pp. 162-172, 1995.
20. J. Wei, P. Saipetch, P. Panwar, D. Chen and B. K. T. Ho, "Volumetric image compression by 3-D discrete wavelet transform," *SPIE Med. Image*, Vol. 2431, pp. 184-194, 1995.
21. M. G. Albanesi and I. De Lotto, "Image compression by the wavelet decomposition," *Signal Processing*, Vol. 3, No. 3, pp. 265-274, 1992.
22. M.Vetterli and J. Kovacevic, *Wavelet and Subband Coding*, Prentice-Hall, Englewood Cliffs, NJ, 1995.
23. G. Strang and T. Nguyen, *Wavelets and Filter Banks*, Wellesley-Cambridge Press, Wellesley, MA, 1996.
24. A. Aldroubi and M. Unser, "Families of multiresolution and wavelet spaces with optimal properties," *Numer. Funct. Anal. Optim*., Vol. 14, pp. 417—446, 1993.
25. C. K. Chui, *An Introduction to Wavelets*, Academic Press, San Diego, CA 1992.
26. A. Cohen, I. Daubechies, and J. Feauveau, "Bi-orthogonal bases of compactly supported wavelets," *Comm. Pure Appl. Math*., Vol. 45, pp. 485—560, 1992.
27. I. Daubechies, *Ten Lectures on Wavelets*, CBMS-NSF Regional Conf. Series in Appl. Math., Vol. 61, Society for Industrial and Applied Mathematics, Philadelphia, PA, 1992.
28. I. Daubechies and W. Sweldens, "Factoring wavelet and subband transformation into lifting steps", *Journal of Fourier Analysis and Application*, No. 4, pp. 245-261, 1998.
29. Oleg S. Pianykh**,** *Lossless Set Compression of Correlated Information*,Ph.D. Disseration, Louisiana State University, August, 1998.
30. Kosmas Karadimitriou, *Set Redundancy, the enhanced compression model, and methods for compressing sets of similar images*, Ph.D. Dissertation, Louisiana State University, August, 1996.
31. W.Sweldens, "The lifting scheme: A custom-design construction of biorthogonal wavelets," *Applied Computational Harmonics Analysis*, Vol. 3, No. 2, pp. 186—200, 1996.
32. A. R. Calderbank, Ingrid Daubechies, Wim Sweldens, and Boon-Lock Yeo, "Wavelet transforms that map integers to integers", *Applied and Computational Harmonics Analysis*, Vol. 5, No. 3, pp. 332—369, July1998.
33. A. Moffat, "An improved data structure for cummulative probability tables," *Software-Practice and Experience*, Vol. 29, No. 7, pp. 647-659, 1999.